Radiation Physics and Chemistry 216 (2024) 111393

Contents lists available at ScienceDirect

Radiation Physics and Chemistry

journal homepage: www.elsevier.com/locate/radphyschem

Feasibility study for the adoption of multi-capsule irradiation protocol in the conduct of k0-based INAA using the GHARR-1 MNSR

George Adu-Okyere [a], Vincent Yao Agbodemegbe [a], Isaac Kwasi Baidoo [a,b], Henry Cecil Odoi [a,b], Edward Shitsi [a,b,*]

[a] Department of Nuclear Engineering, School of Nuclear and Allied Sciences, College of Basic and Applied Sciences, University of Ghana, P.O. Box AE 1, Atomic Energy, Kwabenya, Accra, Ghana

[b] National Nuclear Research Institute, Ghana Atomic Energy Commission, Box LG 80, Legon, Accra, Ghana

ARTICLE INFO

Handling Editor: Dr. Chris Chantler

Keywords:
Reactor characterization
k_0-method
Reference materials
INAA
Multi-capsule irradiation
GHARR-1

ABSTRACT

The Ghana Research Reactor-1 (GHARR-1) is currently a 23 cm length LEU core Miniature Neutron Source Reactor (MNSR) with a 13 % U-235 enrichment having 335 fuel rods, 15 dummy rods and a central control rod for neutron regulation. It has 10 accessible irradiation channels of approximate length of 17 cm and formed part of the shim tray structure which was considered for active routine experiment in the present work. Unlike the routine characterization of the inner irradiation channel of the Ghana Research Reactor- 1 facility which involves mainly the introduction of a single irradiation capsule of length, 5 cm loaded with samples, the present study adopted a multi-capsule scheme in which three (3) capsules each of length 5 cm were introduced into the 23 cm long irradiation channel to scientifically interrogate the feasibility and hence provide a sound basis for extending and improving the accessible irradiation space by 60% during the utilization of the GHARR-1, especially for irradiation involving intermediate and long lived radionuclides. The objective is also to achieve the characterization of neutron spectrum and determine their spatial distribution for close to the full length of the irradiation channel. Validation protocols based on k_0 method were developed through the analysis of some reference materials for a careful study of irradiation, decay and counting scheme which achieved optimum radionuclide selectivity. The overall approach adopted for the flux characterization involves the preparation of flux monitors, packaging of three (3) capsules each of both bare and cadmium cover samples, irradiation at bottom, middle and top spatial demarcation of the irradiation channel, with each demarcation being the region of the 5 cm length of the bottom, middle and top irradiation capsules. Sample counting was undertaken using the HPGe detector after the samples were allowed specific decay time after irradiation and prior to counting. Flux monitors were used for the flux characterization and reference materials were used for the validation protocol. Spectrum acquisition was made possible through the use of the Gamma Vision Software and spectrum parameters (thermal to epithermal neutron flux ration (f), epithermal neutron shaping factor (α), thermal, epithermal, and fast fluxes) were determined. Results obtained showed increasing f-value across the irradiation column as, 18.5 ± 1.7, 21.0 ± 2.2 and 23.0 ± 7.08 respectively from the bottom capsule to the top capsules. The corresponding epithermal neutron shaping factor (α-value) varied as, -0.096 ± 0.029, -0.18 ± 0.036 and -0.20 ± 0.06 from the bottom to the top capsule. The experimental results determined in the bottom, middle and top capsule irradiation column for thermal, epithermal and fast fluxes are $4.60 \times 10^{11} \pm 2.5 \times 10^{10}$, $2.49 \times 10^{10} \pm 5.98 \times 10^{8}$, $9.24 \times 10^{10} \pm 2.2 \times 10^{9}$; $4.21 \times 10^{11} \pm 1.01 \times 10^{10}$, $2.01 \times 10^{10} \pm 4.82 \times 10^{8}$, $4.81 \times 10^{10} \pm 1.15 \times 10^{9}$; and $3.90 \times 10^{11} \pm 9.36 \times 10^{9}$, $1.65 \times 10^{10} \pm 3.90 \times 10^{8}$, $4.82 \times 10^{10} \pm 1.16 \times 10^{9}$ respectively. The validation protocol using standard reference materials and treating each capsule with separate reactor characterization parameters indicated respective z-score distribution within a 95% confidence interval.

* Corresponding author. Department of Nuclear Engineering, School of Nuclear and Allied Sciences, College of Basic and Applied Sciences, University of Ghana, P. O. Box AE 1, Atomic Energy, Kwabenya, Accra, Ghana.

E-mail addresses: dsirgeorge@gmail.com (G. Adu-Okyere), vincevalt@googlemail.com (V.Y. Agbodemegbe), baidooisaac51@yahoo.co.uk (I.K. Baidoo), hencilod@gmail.com (H.C. Odoi), edwardshitsi@yahoo.com (E. Shitsi).

https://doi.org/10.1016/j.radphyschem.2023.111393
Received 28 June 2023; Received in revised form 29 October 2023; Accepted 5 November 2023
Available online 10 November 2023

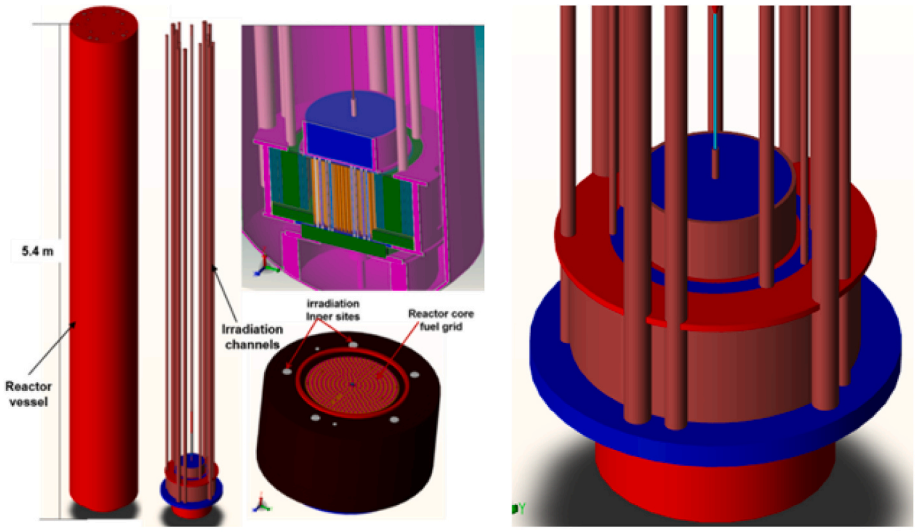

(a) Assembly of GHARR-1 core

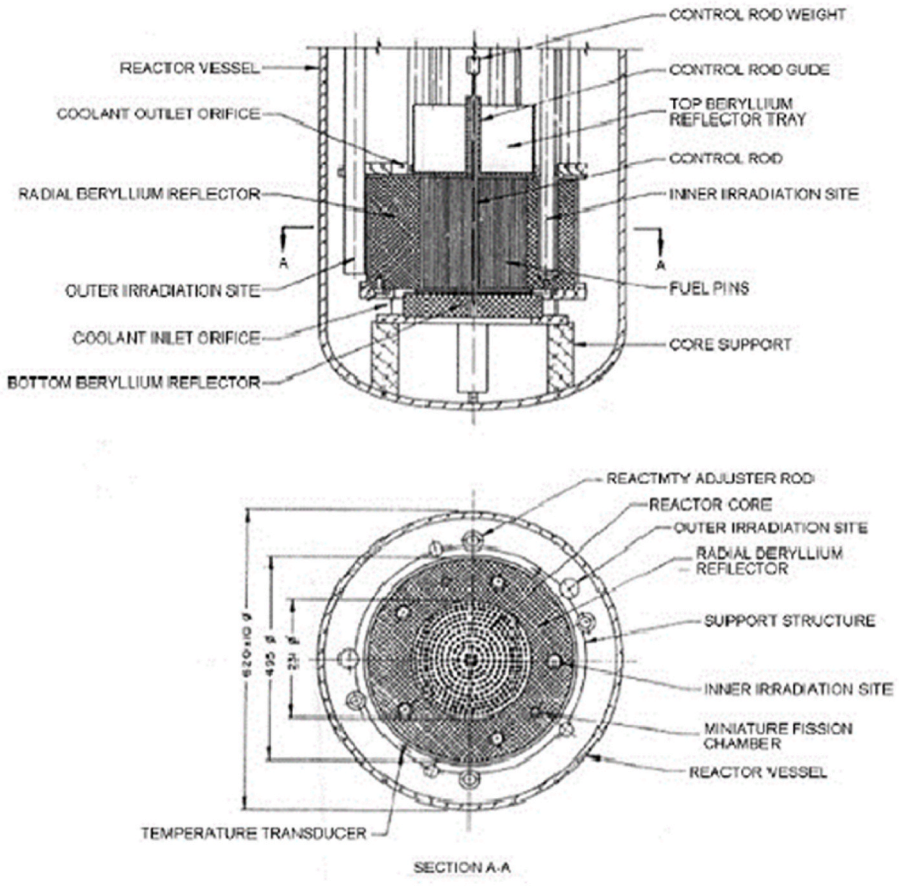

(b) A cross section view through the GHARR-1 core

Fig. 1. GHARR-1 LEU core reactor components.

1. Introduction

The Ghana Research Reactor-1 (GHARR-1) is a miniature neutron source reactor (MNSR) with a maximum thermal neutron flux of 1.0×10^{12} n·cm^{-2}·s^{-1} (the equivalent of 34 kW power), however, operated at half-power (5.0×10^{11} n·cm^{-2}·s^{-1}) for its utilization for routine Neutron Activation Analysis (NAA). Although GHARR-1 is equipped with five inner irradiation channels, only two of them are presently accessible for neutron activation experiments. The remaining three channels are filled with reactivity insertion materials. They also serve as reserved sites for

the insertion of neutron absorbers (Cadmium) for emergency shut down of the reactor when necessary. Neutron activation is routinely performed by irradiating a single capsule loaded with samples per channel. This situation limit the number of samples that could be activated per reactor operation, especially for long-period irradiation.

During these routine utilization, the GHARR-1 irradiation channels are only accessed through the use of a single irradiation capsule of 1.15 cm diameter by 5.6 cm length, although the irradiation column extends as far as 23 cm. This means that, unless extra characterization is carried out to provide sound scientific basis to recommend the use of the remaining accessible space, about 80% of the irradiation column will be unused throughout the lifetime of the reactor.

Several research works conducted at the GHARR-1 facility including (Baidoo et al., 2013) and (Osei et al., 2021) concentrated only on a characterization protocol based on a single capsule in an irradiation channel. The present work was therefore designed to assess the possibility of performing multi-capsule irradiation in a single irradiation channel by developing experimental procedures and also validating a routine irradiation protocols for characterising the active length of the irradiation channel and for possible consideration in the Safety Analysis Report (SAR). The present research endeavour specifically sought to characterise the inner irradiation channel of the GHARR-1 LEU core and determine thermal, epithermal and fast neutron spectra as well as f and α distribution within the irradiation column. The f is thermal to epithermal neutron flux ratio, and α is the epithermal neutron shaping factor which is the measure of the deviation of epithermal neutrons from the ideal 1/E distribution. The present study also sought to calibrate the k_0-IAEA software with the obtained characterisation parameters and conduct validation protocols for the process through the analysis of some reference materials.

The utilization of the GHARR-1 hinges greatly on knowledge of neutron characteristics and their spatial distribution and hence continuous innovation in the methods of neutron flux characterisation are essential in improving results and their timeliness even as such facilities are used for capacity building in the field.

2. Background

2.1. Research reactor neutron characterisation

The 34 kW Ghana Research Reactor-1 (GHARR-1) with 13% enrichment is primarily utilized in the studies of reactor physics, nuclear engineering, nuclear reaction cross-section measurements, neutron activation analysis among others. The current installed Low Enriched Uranium (34 kW MNSR) core is a converted Highly Enriched (HEU), (90.2%, 30 kW) core (Osei, 2017). It has been roughly six years since the conversion was carried out and recent observations and measurements of neutron flux have revealed some distinctive variations in some of the neutron flux parameters as compared to the HEU core, particularly those reported in (Osei et al., 2021). To provide experimenters with the most accurate spectral characteristics of experimental sites and to maintain a high degree of reliable information to carry out reactor experiments and most importantly neutron activation analysis, neutron spectrum characterization of GHARR-1 is the focus of this research work.

The GHARR-1 originally operated on a highly enriched uranium fuel core. However, as part of the US Department of Energy's project on Reduced Enrichment for Research and Test Reactors (Adelfang and Atger, 2006), it was transitioned from high-enriched uranium (HEU) to a low-enriched uranium (LEU) core. According to the GHARR-1 Zero Power Test Report (2016), the GHARR-1 facility successfully undertook the core conversion in 2017. The reactor's maximum thermal neutron flux is 1.0×10^{12} n cm^{-2} s^{-1}. The GHARR-1 facility is used basically for education and training and also for neutron activation analysis.

The main components of the GHARR-1 reactor used in the present study are as depicted in Fig. 1.

In a typical thermal neutron reactor, neutrons are born with varying energies (between 0 and 20 MeV) of which the average energy is about 2 MeV (IAEA, 1990a). These neutrons must undergo slowing down processes (or moderation) to reach thermal energies for subsequent fission reactions with fissile materials. Due to the slowing down processes and other neutron material interactions that take place in the reactor systems (moderator/coolant or shielding materials, etc.), several neutrons of varying energy levels exist in reactor systems. Neutrons with characteristic varying energy levels interact with reactor materials (or experimental samples) in many different ways. These interactions and their corresponding reaction products are strongly dependent on the interacting neutrons' energy. These reasons among others provide the basis for characterizing the neutron spectrum of a reactor system to identify and quantify the different energy types of neutrons available and their characteristic properties. When the properties of neutrons in a specific research reactor are characterized, neutron-material interaction experiments can be carefully designed to enhance optimum quality experimental results. For example, research reactors used for radioisotope productions, material cross-section measurements, or any other type of application require comprehensive knowledge of its characteristic neutron spectrum. In other words, neutron spectrum characterization is required and done in a manner to suit the applications of the reactor type. The NUR and Es-Salam in Algeria are mostly used for neutron-based materials research (Osmani et al., 2023), (Sidi-Ali et al., 2023), whereas South Africa's Research Reactor-I (SAFARI-1) is pioneered in silicon's neutron transmutation doping (manufacturers of the radioisotope molybdenum-99) (Schlünz et al., 2016).

2.2. Neutron activation analysis

Neutron Activation Analysis (NAA) is a multi-elemental method that uses nuclear processes to change stable nuclei into radioactive nuclei and then measures gamma radiation emitted from the reaction product (s) to determine the concentration of the element. The method can be applied to almost all sample types: solids and liquids to determine their elemental composition. The two general NAA procedures employed are classified as: (a) Radiochemical neutron activation analysis which entails putting irradiated materials into a solution such that a chemical separation approach may be used to separate specific trace elements from the more active matrix (Franek and Krivan, 1993), (b) Instrumental neutron activation analysis which entails the irradiation and analysis of samples without any chemical processing before the analysis (Chand et al., 2022). The two classifications are applied based on the irradiation facility, however, at the GHARR-1 facility, instrumental neutron activation analysis is applied.

Instrumental Neutron Activation Analysis is largely the most sensitive, non-destructive and highly selective analytical technique used for multi-elemental analysis today (De Corte and Simonits, 2003). The INAA analytical techniques are used to assess the composition of elements by performing spectroscopy on the produced gamma rays, which are distinct in half life and energy (De Corte et al., 1987a), (De Corte et al., 1979). The quantitative determination of traced elements present is based on the nuclear processes that transform a stable nucleus into radioactive nuclei followed by the estimation or measurement of the reaction products' emission of gamma rays. The identification and quantification are done through the use of gamma-ray spectrometry. Identification and quantification can be accomplished in two ways: (a) The products of irradiation are identified and measured instantaneously upon neutron capture. This is referred to as prompt gamma neutron activation analysis (PGNAA) (Salahi et al., 2022), (b) The resulting radioactive nuclei are measured at a later time in a process known as delayed gamma neutron activation analysis (DGNAA) (Cui and Yang, 2023), (Rodriguez et al., 2021).

In this work, DGNAA was the method of choice. The process of INAA begins by bombarding samples of unknown material of specific mass, along with samples of known elements, in a nuclear reactor (Baidoo et al., 2013). This bombardment (activation) produces specific

radionuclides. These radionuclides emit characteristic gamma rays, which are then measured by radiation detectors (usually germanium detectors) to produce a gamma-ray spectrum. The emitted radiation is specific to the element that emits it, and the amount of radiation detected within an interval (net count) at a particular gamma energy is identified with the amount of the element found in the sample. These results are compared with the results of known concentration samples to determine the concentration of the element(s) in the sample (analyte).

A stable nuclide of atomic mass A and atomic number Z, when exposed to a thermal neutron flux may capture a neutron to produce a radioactive isotope of that element represented by equation (1) (Hien et al., 2023),

$$ {}^{A}_{Z}M + {}^{1}_{0}n = {}^{A+1}_{Z}N + \gamma \tag{1} $$

If W is the weight of the sample used, then the concentration or the amount ρ of a nuclide in the sample is given by equation (2), (Nyarko, 2006):

$$ \rho = \frac{m}{W_i} = \frac{P_A \lambda_i M_i}{\Phi \sigma_i \theta_i N_A \varepsilon_i(E) \gamma_i G (1 - e^{-\lambda_i t_r})(1 - e^{-\lambda_i t_c}) e^{-\lambda_i t_d} W} \tag{2} $$

Equation (2) can be expressed as,

$$ \rho = \frac{m}{W_i} = \frac{(P_A / t_c) M_i}{\Phi \sigma_i \theta_i \gamma_i \varepsilon_i(E) G N_A S C D W} \tag{3} $$

where, m is the mass of an element in a sample, W is weight of a sample, $\varepsilon(E_i)$ is the photopeak detection efficiency for the gamma-ray energy E_i, P_A is the total counts recorded by the detector (the photopeak area), Na is the Avogadro constant, M_i is the molar mass (atomic weight) of the nuclide, σ_i is the cross-section of the nuclide, λ_i is the Decay constant, Φ is thermal neutron flux, θ_i is the isotopic abundance of the target nuclide, G is the abundance of the gamma-ray counted, γ_i is the absolute gamma intensity in the decay of the monitored nuclide, t_r is the exposure time of the nuclide to the thermal neutron flux, t_d is the decay time after irradiation, t_c is the time for counting of the sample. SCDW respectively represents $(1 - e^{-\lambda_i t_r})$ for saturation correction factor S, $(1 - e^{-\lambda_i t_c}) / \lambda t_c$ for measurement correction factor C, $e^{-\lambda_i t_d}$ for decay correction factor D, and weight W of a sample (see equation (2)).

It is required that, instruments used for carrying out qualitative and quantitative analysis of samples during neutron activation analysis are calibrated using Standard Reference Materials (SRM), Certified Reference Materials (CRM) or Reference Materials (RM), which are elements of known concentration (Acharya et al., 2010), (Hamidatou et al., 2012), (Kuběsova' and Kučera, 2011). This is to ensure quality assurance and quality control. In this work, flux monitors of known concentrations and reference materials were used. The flux monitors were used for the flux characterization and the reference materials were used for the validation of protocols.

For reasons of the differences in the quantifications of these materials, three distinct standardization methods, namely, Absolute, Relative and Single Comparator (k_0) methods are available, (Kuběsova' and Kučera, 2011).

It is desirable to be able to use a single comparator or standard for multi-element NAA since the amount of the parent element in the sample can be directly related to each radioisotope observed (Samanta et al., 2021). In lieu of using known weights of standards, multi-element analysis can be performed by irradiating and measuring a single element (comparison) standard. The samples and the single comparator standard are irradiated under the same stable neutron flux conditions. To accomplish this, several methods have been devised; the most widely accepted one is the k_0 method (Baidoo et al., 2013), (Osei et al., 2021). In its early development, the single comparator method, however, employed the proportionality factors called k-factors for the analyte and comparator element after correction for saturation, decay, counting, and weight of the sample, (Acharya et al., 2012). The factors were expressed in k-factors as

$$ k = \frac{M_c \lambda_a \theta_a \varepsilon_a \sigma_{eff,a}}{M_a \lambda_c \theta_c \varepsilon_c \sigma_{eff,c}} \tag{4} $$

where the subscripts "a" and "c" denote both analyte and comparator respectively. However, measured k-factors are only valid for a specific detector, counting geometry, and irradiation facility and also its validity depends on the stability of the irradiation facility (Pomme et al., 1997). To eliminate the inconvenience of continuous re-measuring of k-factors, k_0-factors were introduced, where the effective cross-section (σ_{eff}) and the detector efficiency (ε) are separated from the original k-factors and replaced by

$$ \sigma_{eff} = \sigma_0 \left(1 + \frac{Q_0}{f}\right) \tag{5} $$

Where σ_0 is thermal neutron cross-section, f is thermal epithermal flux ratio and Q_0 is resonance integral/thermal neutron cross-section (I_0/σ_0). The equation describes how an effective cross-section can be divided into the thermal part and part accounting for the activation by epithermal neutrons. The parameter "f" describes the presence of the epithermal neutrons and Q_0 describes the probability of these neutrons activating the nucleus. The k_0 constants then is expressed as,

$$ k_0 = k \frac{f + Q_{0,c}}{f + Q_{0,a}} \tag{6} $$

$$ k_0 = \frac{M_c \lambda_a \theta_a \varepsilon_a \sigma_{0,a} \gamma_a}{M_a \lambda_c \theta_c \varepsilon_c \sigma_{0,c} \gamma_c} \tag{7} $$

The concentration of the analyte is calculated by relating the specific activity of the comparator element and experimentally determined k_0-factor parameters and is given by equation (6) (Acharya and Chatt, 2003), (Baidoo et al., 2013).

$$ k_0 = \frac{\theta_a \sigma_a \gamma_a M_c}{\theta_c \sigma_c \gamma_c M_a} \tag{8} $$

The k_0 constant represents the part of the rate that is independent of the irradiation facility and detector but very essential in the calculation of concentration in k_0-INAA (The k_0-numbers - containing information about the molar mass, isotopic abundance, γ-intensity and 2200 ms^{-1} (n,γ) cross section of the considered isotope - are reactor and detector independent). However, the absence of thermal/epithermal flux ratio (f), resonance integral/thermal neutron cross-section ratio (Q_0), and detector efficiency (ε) in the k_0-factors introduces two separate activities in the utilization of k_0: detector efficiency calibration and reactor neutron characterizations.

The (n, γ) reaction rate (R) measured in per seconds per nuclide for the collision of a nuclide with a neutron is expressed as,

$$ R = \int_0^\infty \sigma(v) \phi'(v) dv = \int_0^\infty \sigma(E) \phi'(E) dv \tag{9} $$

where, E is the energy of the neutron and v is the velocity. E and v can be used interchangeably since E is directly proportional to v ($\frac{1}{2} m_n v^2$, m_n is the mass of a neutron). σ(v) and σ(E) are the neutron cross sections with respect to the velocity (v) and energy (E). The neutron flux per unit interval at velocity (v) and per unit energy at energy (E) are respectively symbolised as $\phi'(v)$ and $\phi'(E)$. Several formalisms or conventions such as Hogdahl, Westcott and Nisle which are based on some neutron characteristics (neutron cross-section and energy distribution) have been adopted in determining R instead of solving the integral (Akaho and Nyarko, 2002). For this study, the Hogdahl convention was adopted.

Table 1
Multi-capsule irradiation protocol.

Position of the capsule	Length range (cm)	Preset flux/ $ncm^{-2}s^{-1}$ at half power (17 kW)	Irradiation Protocol	Irradiation Time/s
Bottom	0 to 5	5.0×10^{11}	The set of capsules labeled "bottom_bare & bottom_Cd" containing the prepared flux monitors was sent in turns into the reactor for both bare and cadmium covered respectively.	5400
Middle	5 to 10	5.0×10^{11}	An empty capsule filled with cotton wool and heat sealed was first sent in each case followed in turns by the capsules labeled "middle bare & midlle_Cd" containing the prepared flux monitors for both bare and cadmium covered respectively.	5400
top	10 to 15	5.0×10^{11}	Two empty capsules filled with cotton wool and heat sealed were first sent followed by the capsule labeled "top_bare & top_Cd" containing the prepared flux monitors for both bare and cadmium covered respectively	5400

3. Methodology

3.1. Multi capsule irradiation protocol for flux characterisation

Table 1 and Fig. 2 show the experimental scheme adopted for flux characterization along the 15 cm length of the 17 cm active length of the inner irradiation channel in the GHARR-1.

3.2. Sample preparation and packaging

The reference materials used consisted of International Soil-Analytic Exchange (121_ISE1 and 131_ISE4) and PTNATIAEA19 (PT_19). 150 mg of each sample was weighed, wrapped in polyethylene vials and then placed inside the irradiation capsules as shown in Fig. 3.

As shown in Fig. 4, each irradiation capsule was sectioned into three planes or columns (i.e., columns A, B and C for the bottom capsule, columns D, E and F for the middle capsule and columns G, H and I for the top capsule). Each of the columns was filled with three samples of the same reference materials. For instance, the bottom capsule was filled with PT_19, 121_ISE1 and 131_ISE4 at columns A, B, and C respectively in addition to a gold monitor which was affixed in between samples in each column. The sample packaging procedure was replicated for the other two capsules (middle and top). In all, nine reference materials were packaged into each capsule and three gold monitors making a total of twelve samples in each capsule.

3.3. Preparation and packaging of flux monitors (CRMs – wire)

Preparation of flux monitor samples was done by weighing pieces of each flux monitor (i.e. Gold foil and also Zirconium, Cobalt and Iron wires which were available for the experiment using an electronic micro-balance (ACCULAB) (See Table 2). The weighted masses of the flux monitors ranged between 15 and 25 mg. Fig. 5 is a picture frame showing some flux monitor samples and also the electronic balance used. The micro-balance measures weight of samples up to a maximum of 120 g with a 0.0001 g deviation. For a specified material's percentage purity, the actual mass of a given flux monitor is determined as, (De Corte et al., 1987b).

$$\text{The actual mass of sample} = \frac{\text{Total mass weighed}}{100\%} \times \%\text{purity} \tag{10}$$

The Hogdahl convention requires two (2) sets of activation of flux monitors. A set of the monitors irradiated under the 1 mm thick cadmium (i.e., cadmium cover irradiation), and the other set is irradiated without the cadmium cover (bare irradiation). Two sets of packaging were done, one under cadmium and the other bare. In the case of the cadmium-covered packaging, all the designated (weighed) flux monitors were packed into the small capsule and then placed inside the cadmium cylinder with the top and bottom cover. The cadmium cylinder and the smaller capsule were further placed into the irradiation capsule as shown in Fig. 6. However, for the bare irradiation, the wires were packed into a small capsule and then placed inside the irradiation capsule. The packaging was repeated for two more capsules, for a total of six packaged flux monitors (i.e., three bare and three cadmium covered).

The dimension of the smaller capsule is 1.5 cm by 0.5 cm in height by diameter respectively. The irradiation capsule has dimensions of 5 cm by 1 cm height by diameter respectively. The smaller capsule was used for sample packaging and not for direct irradiation and in most cases, used in addition to the irradiation capsule. A cadmium cylinder was also used in addition to the capsules. The cadmium cylinder was prepared by

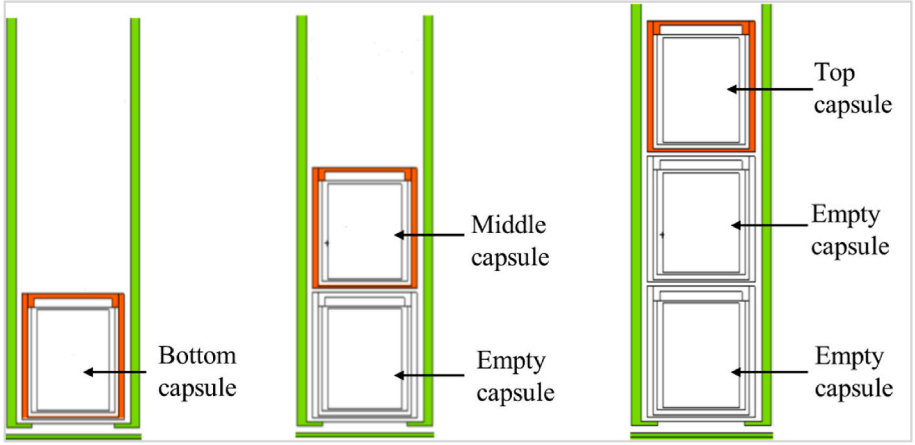

Fig. 2. Multi-capsule irradiation protocol.

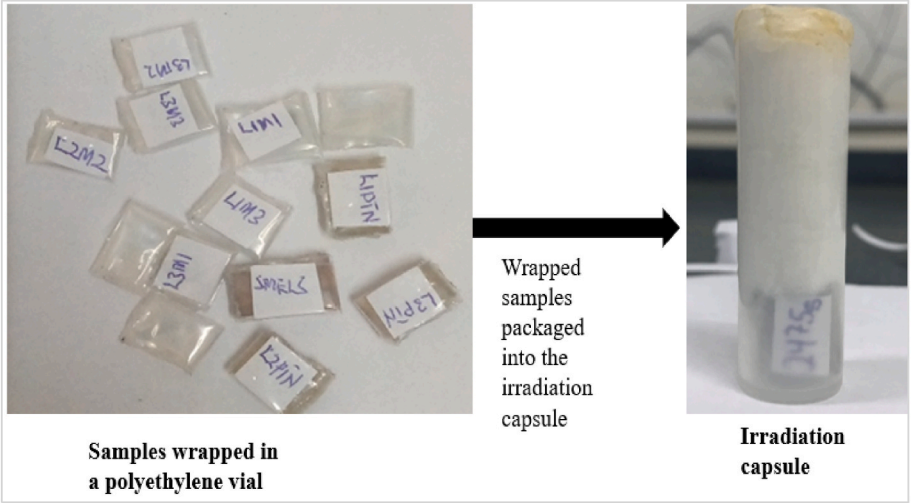

Fig. 3. Multi-capsule irradiation sample preparation.

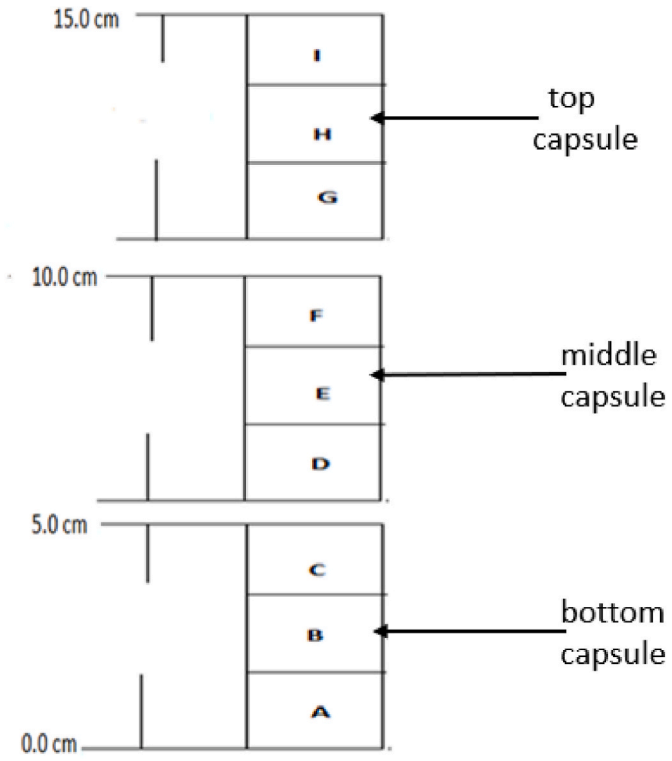

Fig. 4. Multi-capsule irradiation sample packaging scheme in irradiation capsules.

Table 2
Materials' physical characteristics and catalog numbers (van Sluijs et al., 2014).

Materials (wires)	Purity	Diameter (thickness)	Catalog number
Gold	0.1%Au–Al	0.1 mm	ERM-EB530A
Cobalt	0.1%Co–Al	0.1 mm	IRMM-527RB
Zirconium	Zr–97.2%	0.55 mm	ZR566814
Iron	Fe–99.5%	0.05 mm	FE525215

cutting a 1 mm thick cadmium plate into a rectangular shape in accordance with the dimensions of the smaller capsule (i.e., 3 cm by 0.8 cm height by diameter). The plate was then folded into a cylinder with both top and bottom covers.

3.4. Irradiation and counting of flux monitors

Each set of the monitors (CRM-wire) was irradiated for 2 h and left to decay overnight (i.e., about 10–16 h decay) and counted for 2 h. In the case of the reference materials, the samples were irradiated for a maximum of 3 h at half power (17 kW) which corresponded to a preset flux of 5×10^{11} ncm^{-2}s^{-1} from the reactor control console. The samples were allowed a four-day delay time following the irradiation and counted for 900 s and again counted for 7200 s after decaying for seven more days. The HPGe detector was used for all measurements, which were carried out at a 50 mm source-detector distance. It was advisable to irradiate flux monitors and reference materials separately because they were of different material types (i.e. metal flux monitors and non-metal reference materials). Also, the irradiation times for the flux monitors and reference materials were different. A stable neutron flux was used for the irradiations.

The detector system used in the present work is as shown in Fig. 7. The system is made of N-type High Purity Germanium (HPGe-coaxial type). At a gamma energy (γ-energy) of 1332 keV of ^{60}Co, the detector's relative efficiency is 40%, and its energy resolution is 1.8 keV. The detector is connected via the multi-channel analyzer to a computer system, with Genie-2000 gamma spectrum evaluation software. The detector efficiency calibration curve was done using the europium-152 (Eu-152) point source. All gamma spectrum acquisitions were done at a counting geometry of 50 mm. It should be noted that each level of the counting geometry has its corresponding efficiency.

3.5. Flux monitors and reference materials

In this work, Flux monitors and Reference Materials were used. The Flux monitors were used for flux characterization and the Reference materials were used for the validation protocols. The characterization materials were obtained from the Joint Research Centre (JRC), Institute for Reference Materials and Measurement (IRMM). Tables 2 and 3, respectively, list the materials along with their associated physical and nuclear characteristics as well as their catalog numbers.

3.6. Determining reactor neutron parameters

The cadmium ratios, thermal to epithermal neutron flux ratio (f), epithermal neutron shaping factor (α), thermal neutron flux, epithermal neutron flux, and fast neutron flux were the parameters of relevance or

Fig. 5. Flux monitor samples and electronic weighing balance.

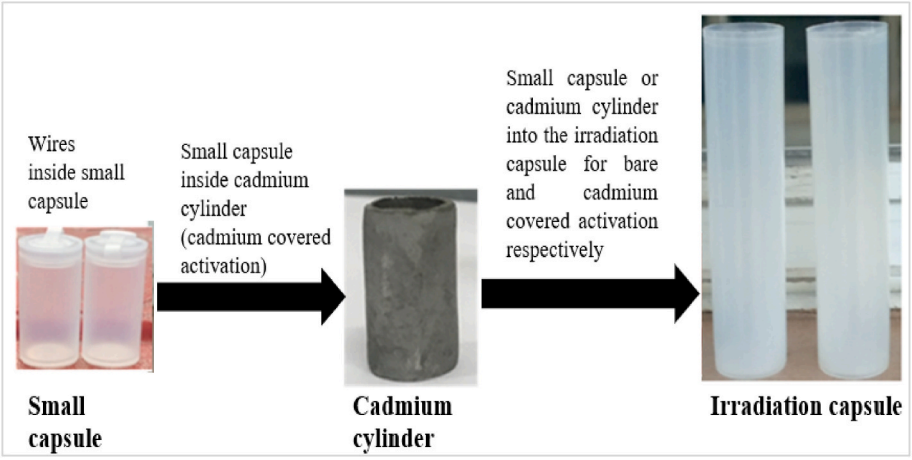

Fig. 6. Sequence for flux monitor packaging.

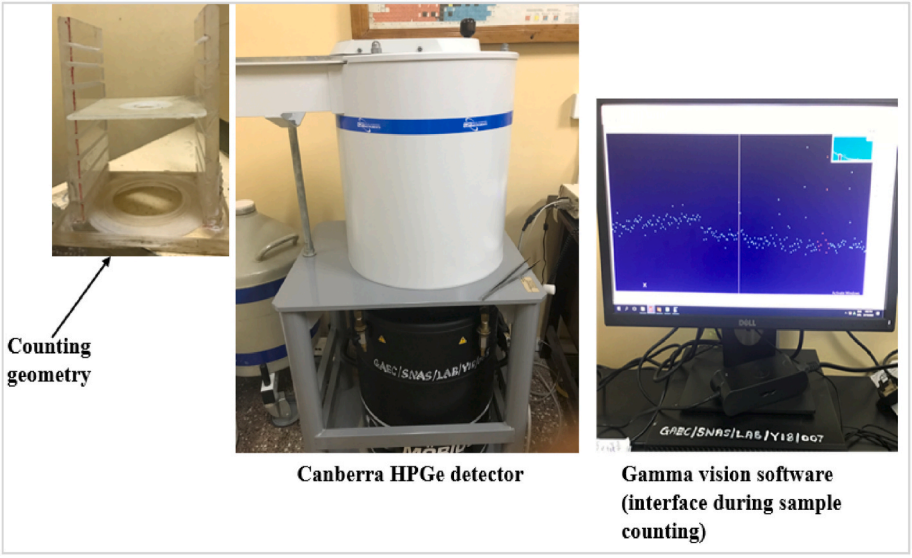

Fig. 7. GHARR-1 spectroscopy system for sample data acquisition.

Table 3
Nuclear Properties of the Materials and their Respective Reactions used for Neutron Fluence Rate Measurement (IAEA, 1990b).

Reaction	Reaction cross-section (barns)	Resonance integral (barns)	Isotopic abundance	Half-life (days)	Energy (keV)	Gamma emission (%)
^{197}Au (n, γ) ^{198}Au	98.65	1550.0	1.000	2.70	411.80	95.58
^{59}Co (n, γ) ^{60}Co	37.13	74.0	1.000	1923.55	1173	99.85
^{94}Zr (n, γ) ^{95}Zr	0.0530	0.268	0.028	2.69775	724.20 + 756.7	44.27
^{54}Fe (n, p) ^{54}Mn	82.5×10^{-3}	1.1×10^{-3}	0.058	312.12	834.84	56.40

interest in this characterization analysis. These parameters are essential for k_0-standardization and the k_0-IAEA software calibration. The reaction rate according to the Hogdahl approach is given as (Osei, 2017):

$$R = \int_0^{vCd} \sigma(v)\varphi'(v)dv + \int_{E_{Cd}}^{\infty} \sigma(E)\varphi'(E)dE \tag{11}$$

Using Gold (Au) as a standard, the concentration, ρ, of an element in a sample was calculated using equation (12). Equation (12) was obtained from eqn (11) after thorough derivation based on Hogdahl convention (Baidoo et al., 2013), (Osei et al., 2021), (Osei, 2017), (Nyarko, 2006).

$$\rho = \frac{\left(\frac{P_A/t_c}{SCDW}\right)_i}{\left(\frac{P_A/t_c}{SCDW}\right)_{Au}} \frac{1}{k_0} \frac{f + Q_0(\alpha)_{Au}}{f + Q_0(\alpha)_i} \frac{\varepsilon_p(E_{Au})}{\varepsilon_p(E_i)} \tag{12}$$

where P_A is the photopeak area, t_c is the counting time, ε_p is the photopeak efficiency of the detector. SCDW are the factors accounting for Saturation during irradiation, Counting, Decay after irradiation and Weight of nuclide of interest respectively. k_0 factors is given as,

$$k_0 = \frac{\theta_i \sigma_i \gamma_i M_{Au}}{\theta_{Au} \sigma_{Au} \gamma_{Au} M_i}$$

Therefore, from equation (12), f and α are the parameters of interest and the steps outlined below were used in their determination. $Q_0(\alpha)$, the ratio of the non-ideal resonance integral to the thermal cross-section, is given as,

$$Q_0(\alpha) = \frac{Q_0 - 0.429}{E_r^{-\alpha}} + \frac{0.429}{(2\alpha + 1)E_{Cd}^{\alpha}} \tag{13}$$

Based on the Cadmium ratio (R_{Cd}) technique or method, the thermal-epithermal flux ratio (f) was calculated as:

$$f = \frac{\phi_{th}}{\phi_{epi}} = Q_0(\alpha)(R_{Cd} - 1) \tag{14}$$

ϕ_{th} and ϕ_{epi} are the thermal flux and epithermal flux respectively. The cadmium ratio (R_{cd}) is determined as,

$$R_{Cd} = \frac{A_b}{F_{Cd} A_{Cd}} \tag{15}$$

A number of ways or methods (i.e., cadmium ratio dual monitor, cadmium ratio multi-monitor and bare monitor triple method) for applying the cadmium ratio concept in determining f and alpha are available. Using the dual monitor (Au and Zr) method by considering the reaction ^{197}Au (n, γ)^{198}Au and ^{94}Zr (n, γ)^{95}Zr, f and α was iterated from equation (14) with the assumption that, in the same irradiation column or site, $f_{Au} = f_{Zr}$. Equation (14) can therefore be re-written as,

$$(Q_0(\alpha)(R_{Cd} - 1))_{Au} = (Q_0(\alpha)(R_{Cd} - 1))_{Zr} \tag{16}$$

By factoring the thermal (G_{th}) and epithermal (G_{epi}) self-shielding factors for the nuclides (Au and Zr) into equation (16), f and α were determined from equation (17).

$$f_{Au} - f_{Zr} = \left[Q_0(\alpha).\frac{G_{epi}}{G_{th}}(R_{Cd} - 1)\right] - \left[Q_0(\alpha).\frac{G_{epi}}{G_{th}}(R_{Cd} - 1)\right] = 0 \tag{17}$$

Having determined R_{Cd} for Au and Zr, a starting value for α was assumed and the iteration was carried out while being watched for convergence. From the excel sheet used for the iteration, the f and α were obtained at the point of convergence.

3.6.1. *Thermal neutron fluence density determination*

The thermal neutron flux was determined by activation of the monitor foils (Au and Co). Irradiating each of the foils for bare and cadmium covered, the reaction rate (R) per atom which is a result of the exposure of the nuclide to mixed thermal and epithermal neutrons field was calculated as,

$$R = R_s + R_{s,cd} \tag{18}$$

where R_s and $R_{s,Cd}$ are respectively the sub-cadmium (thermal) and Cadmium-covered (epithermal) reaction rates. From equation (18), R is given as,

$$R = G_{th}.\sigma_0 + G_e.I_0(\alpha).\phi_e \tag{19}$$

where, $\boldsymbol{\sigma}_0$ is the cross section of the nuclide, G_{th} is the thermal shelf-shielding factor, G_e is the epi-cadmium neutron self-shielding factor, $I_0(\alpha)$ is the non-ideal resonance integral, ϕ_e is the epithermal flux.

By re-arranging equations (18) and (19), the thermal (sub-cadmium) reaction rate, i.e. (R_{th} or R_s) was related to epithermal (Cadmium covered) reaction rate, i.e. (R_e or $R_{s,Cd}$) as

$$R_s = R - R_{s,Cd} = R - \frac{R_{s,Cd}}{F_{Cd}} = G_{th}\sigma_0\phi_{th} \tag{20}$$

The thermal fluence rate of the foil was calculated as:

$$\phi_{th} = \frac{1}{G_{th}\sigma_0}\left(R - \frac{R_{s,Cd}}{F_{Cd}}\right) \tag{21}$$

where,

$$RorR_{s,Cd} = \frac{\left(A_{sp}orA_{sp,Cd}\right)\exp(\lambda t_d)}{[\varepsilon N_0(1 - \exp(-\lambda t_i))]} \tag{22}$$

which is the reaction rate per target atom for bare (R) or Cadmium-covered ($R_{s,Cd}$) irradiation. ε is the efficiency of the detector for a specific gamma peak at a specific counting geometry, t_i is the irradiation time, t_d is the decay time (elapsed time from the end of the exposure period to the time of counting) and N_0 is the original number of atoms of the nuclide to be activated. From equation (22), the specific activity obtained for a bare (A_{sp}) or Cadmium covered ($A_{sp,Cd}$) irradiation is given as

$$A_{sp}orA_{sp,Cd} = \frac{N_p/t_m}{WSDC} \tag{23}$$

where N_p is net photopeak, t_m is the measuring time (Mensimah et al., 2011), (Sogbadji et al., 2011), (Karadag et al., 2003).

3.6.2. *Epithermal neutron fluence density determination*

In this work, the epithermal flux was determined from equation (24)

$$f = \frac{\phi_{th}}{\phi_{epi}} \tag{24}$$

With f determined from equation (17) based on the iteration and ϕ_{th}

Table 4
Neutron flux characterization parameters determined in the inner irradiation channel at bottom, middle and top capsule positions.

Capsule Position	Reference	R_{cd}		f	α	φ_{th}	φ_{epi}	φ_f
		^{97}Au	^{94}Zr					
Bottom Capsule	*EXP. (Present Work)*	*2.21*	*3.00*	*18.5 ± 3.7*	*−0.096 ± 0.029*	*$4.6x10^{11}\pm1.11x10^{10}$*	*$2.49x10^{10}\pm5.98x10^{8}$*	*$9.24x10^{10}\pm2.2x10^{9}$*
	EXP. (Baidoo et al. (Baidoo et al., 2013)*)*	*2.08*	*3.45*	*18.8*	*−0.048*	*$5.12x10^{11}$*	*$2.47x10^{10}$*	*$2.49x10^{10}$*
	EXP. (Osei et al. (Osei et al., 2021)*)*	*2.02*	*3.51*	*16.8*	*−0.039*	*$5.02\ x10^{11}$*	*$2.98\ x10^{10}$*	*$10.4\ x10^{10}$*
Middle Capsule	*EXP. (Present Work)*	*2.10*	*2.06*	*21.0 ± 4.2*	*−0.18 ± 0.036*	*$4.21x10^{11}\pm1.01x10^{10}$*	*$2.01x10^{10}\pm4.82x10^{8}$*	*$4.81x10^{10}\pm1.15x10^{9}$*
Top Capsule	*EXP. (Present Work)*	*2.63*	*2.04*	*23.0 ± 7.08*	*−0.20 ± 0.06*	*$3.90x10^{11}\pm9.36x10^{9}$*	*$1.65x10^{10}\pm3.90x10^{8}$*	*$4.82x10^{10}\pm1.16x10^{9}$*

* **R_{Cd}:** Cadmium ratio.
*__α:__ Measure of the deviation of epithermal neutrons from the ideal 1/E distribution.
*__f:__ Thermal-epithermal flux ratio.
* **φ_{th}:** Thermal neutron flux ($ncm^{-2}s^{-1}$).
* **φ_{epi}:** Epithermal neutron flux ($ncm^{-2}s^{-1}$).
* **φ_f:** Fast neutron flux ($ncm^{-2}s^{-1}$).

determined from equation (21), the epithermal flux density (ϕ_{epi}) was calculated as (Mensimah et al., 2011), (Sogbadji et al., 2011), (Jovanovic et al., 1988), (IAEA, 1970):

$$\phi_{epi} = \frac{\phi_{th}}{f} \tag{25}$$

3.6.3. Fast neutron fluence density determination

The fast neutron fluence density (ϕ_f) was determined from the activity of irradiated Iron (wire), based on reaction (^{54}Fe (n, p) ^{54}Mn). Usually, the fast neutron spectrum or flux is defined as,

$$\phi_f = \int_{0.5}^{10} \phi(E)dE \tag{26}$$

The limit of integration represents fast neutron energy in the range 0.5 MeV–10 MeV. The capture cross-section of the flux monitor (iron) presented for fast neutrons interaction is 81.7 mb. The rate of fast neutrons interaction with the atom (flux monitor) is given by the equation

$$R(t) = N_t \int_{0.5}^{10} \Phi(E)\sigma_f(E)dE = N_T\sigma_f\Phi_f \tag{27}$$

where, $N_t = \theta.w.N_A/M$, is the total number of the nuclides of interest in the target (Mensimah et al., 2011); (Sogbadji et al., 2011); (Karadag et al., 2003). By rearranging equation (27) and introducing gamma emission probability for the produced radionuclide (^{54}Mn), the fast neutron flux density was calculated from equation as,

$$\phi_f = \frac{A_{sp}\ \exp\ (\lambda t_d)}{\left[\varepsilon N_0 \theta\gamma\sigma_f(1-\exp(-\lambda t_i))\right]} \tag{28}$$

where, N_0 is the initial number of atoms of the nuclide to be activated (Fe), θ is the isotopic abundance, ε is the efficiency of the nuclide, $\boldsymbol{\sigma}_f$ is the capture cross section and t_i and t_d are the irradiation and decay times respectively (Mensimah et al., 2011), (Sogbadji et al., 2011), (Kumar et al., 2017), (Khattab, 2007), (Kubešová and Kucera, 2012), (Baidoo, 2012).

4. Results and discussion

4.1. Neutron spectrum parameters

The neutron spectrum parameters such as the cadmium ratios (R_{cd}), the measure of the deviation of epithermal neutrons from the ideal 1/E distribution (α), the thermal-epithermal flux ratio (f), the thermal, epithermal and fast neutron fluxes determined inside each irradiation capsule positioned at the bottom, middle and top in the inner irradiation channel as shown in Fig. 4 are as presented in Table 4.

The results obtained for the bottom capsule were compared with similar experiments performed by (Baidoo et al., 2013) and (Osei et al., 2021).

It could be observed from the results presented in Table 4 that, within the limit of the specified uncertainty, there is general agreement of the present parameters obtained with the results from the study conducted by Baidoo et al. (2013). However, the GHARR-1 HEU core other than the present LEU core, after the GHARR-1 core conversion was used in their work and the experiment was performed at a reactor power of 15 kW, whiles the present work, was conducted at a reactor power of 17 kW. It could be observed that the thermal-epithermal flux ratio results agree fairly in both works. However, a relatively large difference in the α-value [(i.e., −0.096 and −0.048 respectively for this work and that of (Baidoo et al., 2013) was observed. The relatively large difference in the α-value might be due to the variation in the Cadmium Ratio estimated from the activation/irradiation of bare and cadmium covered radioisotopes at reactor powers of 15 kW and 17 kW for HEU and LEU cores respectively. Large variations in alpha value for specific reactor facilities including large associated uncertainties were also reported in the work of (Kubešová and Kucera, 2012).

The α-value gives information about how hardened or softened the spectrum is (i.e., the more negative the α-value, the more hardened the spectrum). It is indicated from the comparison that the LEU spectrum is more hardened than the HEU. Furthermore, a relatively high thermal flux (5.12×10^{11}) was recorded by Baidoo et al. (2013) as compared to the thermal flux (4.6×10^{11}) recorded in the present work. Comparatively, value of the epithermal flux was also in agreement with that obtained in the work by Baidoo et al. (2013). In addition to the relatively high thermal flux obtained in the present work, the high fast neutron flux measured in this work further suggests a hardened neutron spectrum (i.e., the neutron spectrum is shifted to high energies) after the core conversion from the HEU to the present LEU.

It is important to indicate that the comparison of the present experimental results to that recently published by (Osei et al., 2021), serves a suitable means of validating the multi capsule irradiation protocols introduced in this work. With the exception of large deviation present in the alpha (α) value obtained, a general agreement between the two results within reasonable deviations specific to the neutron parameter could be observed. Comparing results of the neutron flux parameters at the three (3) positions studied, it could be clearly remarked that the thermal-epithermal flux ratio (f) increases axially along the core (i.e., f increases as one moves away from the bottom of the core). Similarly, the α - value also decreases (i.e., α becomes more negative) as one moves away from the bottom of the core. The trends of this observations are depicted in Fig. 8.

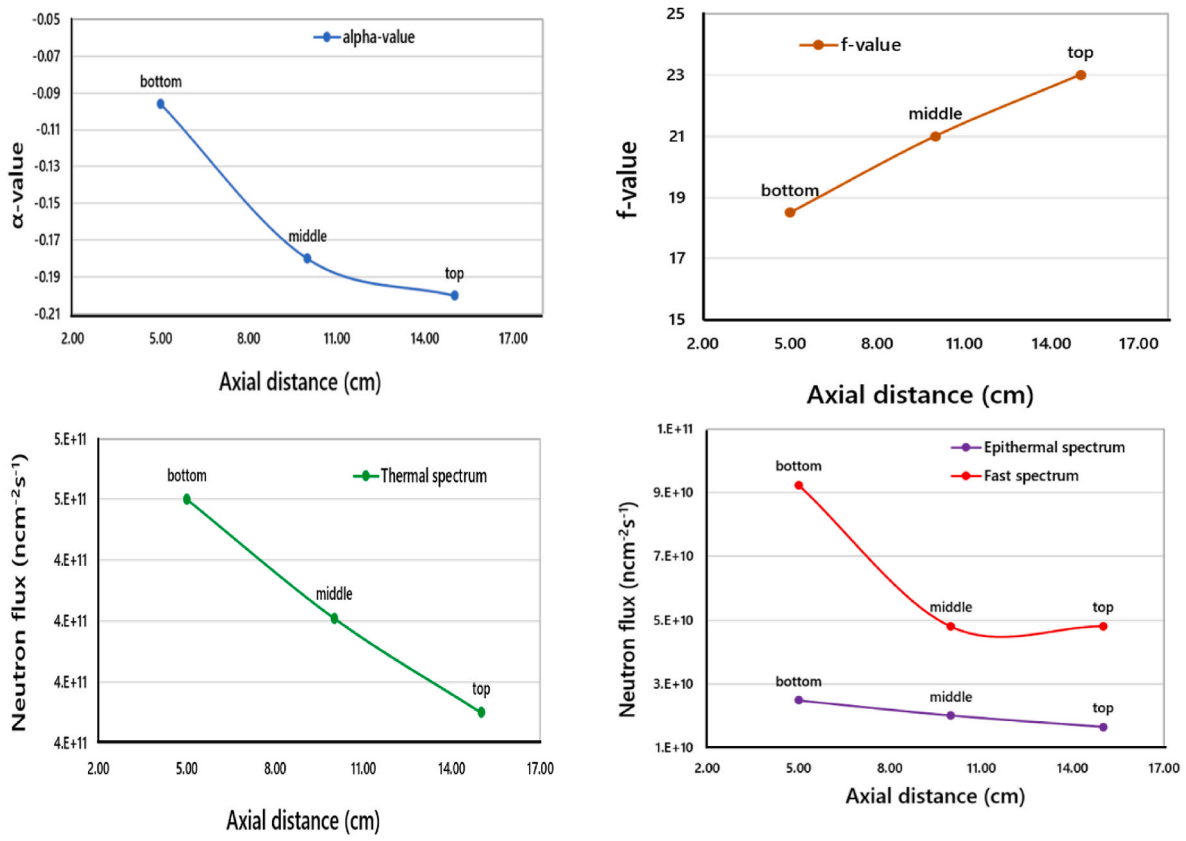

Fig. 8. Plots of α, f, Thermal, Epithermal and Fast Neutron Flux Measured at the Three Capsules Positions in the Inner Irradiation Column.

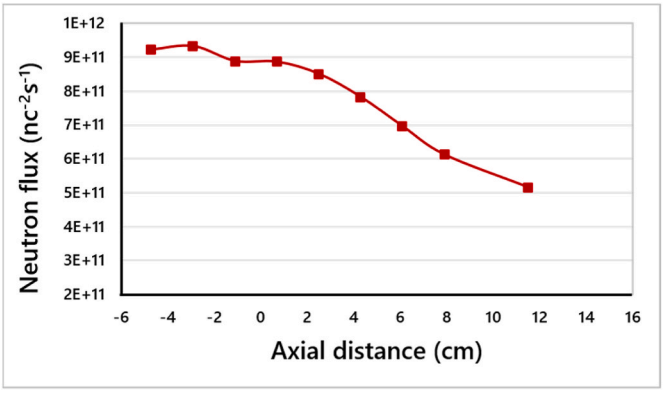

Fig. 9. Axial neutron flux distribution in the LEU inner irradiation channel.

Generally, as f increases and α decreases (α becoming more negative), the neutron flux also decreases indicating the hardening of the spectrum as the capsule location in the irradiation location moves away from the bottom of the reactor core.

The total neutron flux in the axial direction from the bottom of the Inner Irradiation Channel was also determined in this work. Nine monitors were used to determine the axial flux fluctuation. Three capsules were packed with samples and three flux monitors (Au) were attached in between samples in each capsule. Fig. 9 presents the axial flux distribution.

The horizontal axis of Fig. 9 indicates the position of the flux monitors along the vertical axis of the inner irradiation column. From the bottom of the channel up, the plot depicts a perpetually reducing neutron flux density. The fluctuation observed along the axial profile of the neutron flux is similar to findings obtained from an MCNP simulation study carried out by (Baidoo et al., 2013). Detailed analysis of neutron self-shielding was not the focus of this work. It is however anticipated that neutron self-shielding could also contribute to the trend in Fig. 9. This is because each flux monitor was sandwiched between the actual samples (soil matrix). It is, therefore a worthwhile recommendation that further work be done to ascertain and quantify the contribution of neutron self-shielding for different sample matrices.

Nonetheless, the determined elemental concentrations obtained from the analysis of samples for the validation of the multi capsule irradiation protocol did not show significant effect from the neutron self-shield as the result across each capsule was consistent with the certificate results. However, the observed variations in neutron flux density across the irradiation column are very much significant and hence require correcting and accounting for non-uniform neutron flux distribution from the bottom of the irradiation channel to the top channel.

It is, therefore, suggestive that a full implementation of the multi-sample and multi-capsule irradiation protocol will require an adequate neutron flux monitor (Gold wire) for routine neutron flux determination across the irradiation column. Its implementation in the k_0-software will require that the software provides a submenu to define sample position (column and row) and once monitors are affixed to samples in these positions, the monitors are analyzed and their thermal flux densities are mapped for the samples and used accordingly for concentration calculation. Thus making accounting for thermal neutron attenuation and non-uniform sample activation in the k_0-software quite appreciable. Here the emphasis is placed on using adequate flux monitors to map out the seeming fluctuation in neutron flux across the bottom to the top of the capsule. One of the key findings in this work is having identified this trend and correcting for its impact through the use of the k_0-software. Yet again indicating the focus of this work towards achieving the optimum utilization objective set up for this work.

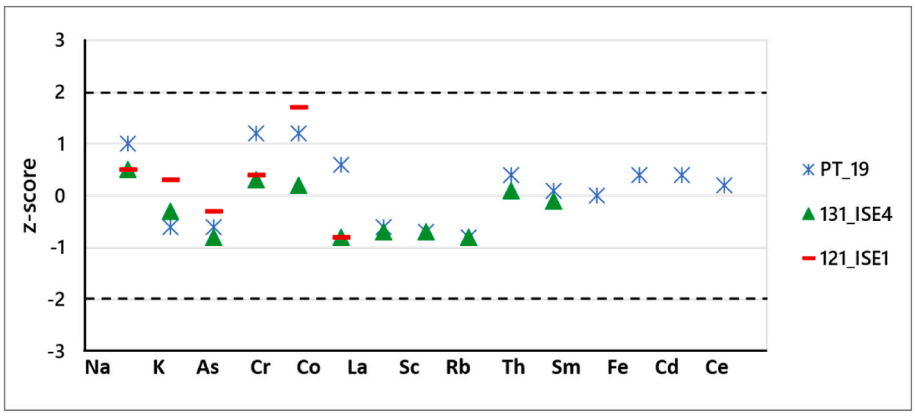

Fig. 10. Z_Score distribution of analytical result obtained at the bottom irradiation capsule.

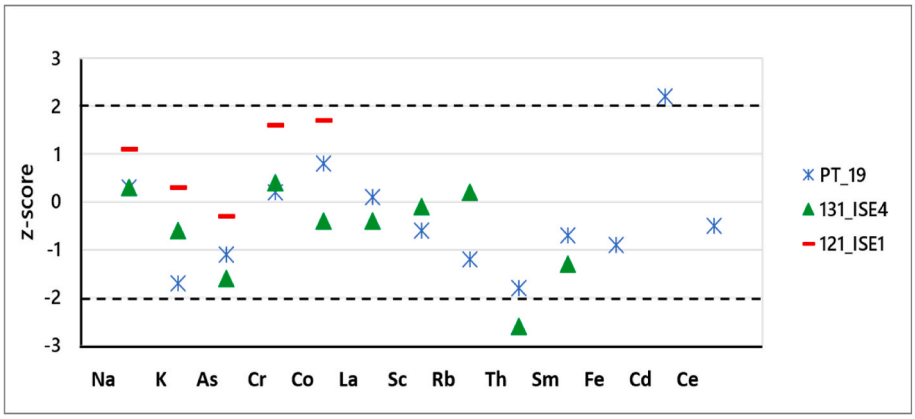

Fig. 11. Z_Score distribution of analytical result obtained at the middle irradiation capsule.

4.2. Validating the multi-capsule irradiation protocol

It is worth noting that the assessment of the quality of the experimental parameters can be determined from its actual implementation in the k_0-software and its application for elemental quantification.

The reactor neutron characterization was validated through the analysis of reference materials [i.e., International Soil-Analytic Exchange (121_ISE1 and 131_ISE4) and PTNATIAEA19: PT_19] via the k_0-IAEA software. In performing the analysis, three distinct characterization sites were demarcated based on the relative position of the irradiation capsule (i.e., bottom, middle and top) and their corresponding parameters (thermal, epithermal and fast fluxes, f and α) used in characterizing each site determined. In all, twenty (20) samples were analyzed, however, nine (9) are presented and discussed in this section. The reference materials were analyzed by comparing their analytical results obtained to their reference certificate using Z_Score. The Z_Score is defined based on the Normal Distribution Approximation (NDA) model as the difference between the reported value and the calculated mean values divided by the standard deviation calculated and expressed as (Baidoo et al., 2013), (Baidoo, 2012):

$$Z_{Score} = \frac{X - X_{mean}}{S_d} \tag{29}$$

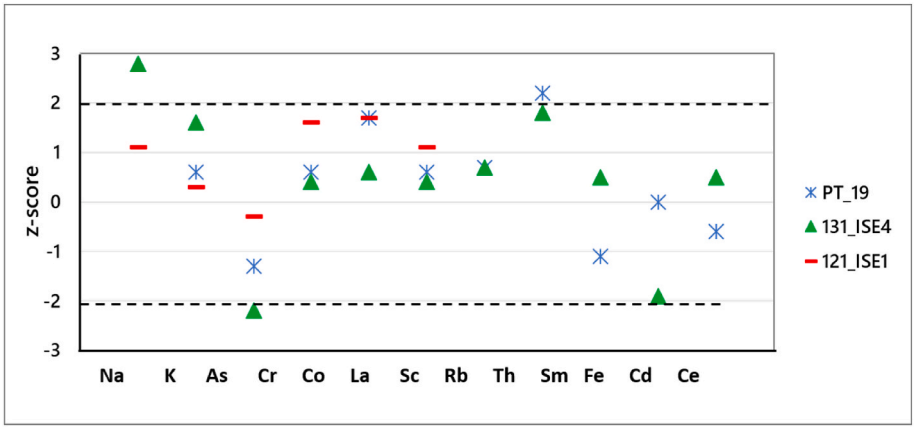

Fig. 12. Z_Score distribution of analytical result obtained at the top irradiation capsule.

where, X is the reported value, X_{mean} is the mean of all values calculated with the Normal Distribution Approximation (NDA) model and S_d is the standard deviation calculated with the NDA model.

However, during sample analysis, the k_0-software automatically calculates the Z_Scores with its corresponding concentration for each element of interest. In this work, the accuracy of the measured concentration or the analytical value was assessed based on the absolute value of the Z_Score as, $|z,z'| \leq 2$. This means that, the analytical results were considered as satisfactory performance (95% confidence interval) if the Z_Score distribution is within the range specified. However, with Z_Score distribution outside this specified range, the results were considered either questionable or unsatisfactory performance. Figs. 10–12 present the Z_score distribution of the analytical results obtained for the Bottom, Middle and Top Irradiation Capsules.

From the distribution, it is observed that all the analytical results obtained for the bottom capsule as in Fig. 10 were distributed within the 95% confidence interval. Determination for two (2) samples for the middle capsule (Fig. 11) fell outside the 95% z_score distributions whiles three (3) data points were out of the 95% z_score distribution range for the analyses conducted in the top irradiation capsule as depicted in Fig. 12. It should be emphasized that in each of the three cases (top, middle and bottom), the results presented were randomly distributed within the range of −2 to 2 indicating that there was no systematic error. Also, in the cases where the results fell outside $|z,z'| \leq 2$, the data points were satisfactory and acceptable, i.e., $|z,z'| \leq 3$. The observed percentage of the analytical results that were found outside the 95% confidence interval could be attributed partly to the sample preparation approach or procedure and perhaps the mass of the sample weighed.

5. Conclusions

The characterization of neutron flux spectrum and the assessment for the use of the remaining available space other than that occupied by a single irradiation capsule in the conduct of neutron activation analysis in the active 17 cm long inner irradiation channel especially for intermediate and long irradiation requirement was undertaken through the adoption of a multi-capsule irradiation scheme developed in the present work. Flux characterisation and analytical measurement of sample were carried out in three (3) irradiation capsules introduced into the inner irradiation channels at the bottom (normal), middle and top positions using the scheme developed in the present work. Cadmium ratios, a measure of the deviation of epithermal neutrons from the ideal 1/E distribution (α) and thermal-epithermal flux ratio (f) were determined for the three capsules as well as the thermal, epithermal and fast neutron fluxes. From the k_0-IAEA software sample analysis (i.e., the validation of the characterization process), the elemental concentrations determined were accessed based on a Z_Score distribution: $|z,z'| \leq 2$. In all about 15 elements (long-lived) were determined and quantified based on the multi-capsule irradiation scheme. About 90% of the resulting data points were within the accepted range: $|z,z'| \leq 2$, i.e., 95% confidence interval. The results indicated that a multicapsule irradiation approach is generally feasible. However, a separate characterization may be required for the top capsule, while a single generalized characterization will be valid for the bottom and the middle positions.

It is recommended that a study to be carried out to further interrogate the impact of neutron self-shielding on results from multi-capsule irradiation scheme applied in the present work.

Author statement

All the authors participated in obtaining the experimental results presented and writing of this paper.

Declaration of competing interest

The submitted manuscript for review has no conflict of interest in one form or the other in relation to similar research studies in the literature.

Data availability

Data will be made available on request.

Acknowledgement

The authors acknowledge the technical supports from Scientists and Technicians at the Ghana Research Reactor-1 (GHARR-1) facility of the Ghana Atomic Energy Commission (GAEC).

References

Acharya, R., Chatt, A., 2003. Characterization of the Dalhousie University SLOWPOKE-2 reactor for k0-NAA and application to medium-lived nuclides. J. Radioanal. Nucl. Chem. 257 (3), 525–529.

Acharya, R., Swain, K.K., Reddy A V R, A.V.R., 2010. Analysis of SMELS and reference materials for validation of the k0-based internal monostandard NAA method using in-situ detection efficiency. Nucl. Instrum. Methods Phys. Res. 622, 411–414. https://doi.org/10.1016/j.nima.2009.12.072.

Acharya, R., Holzbecher, J., Chatt, A., 2012. Determination of k0-factors of short-lived nuclides and application of k0-NAA to selected trace elements. Nucl. Instrum. Methods Phys. Res. 680, 1–5. https://doi.org/10.1016/j.nima.2012.04.001.

Adelfang, P., Atger, A., 2006. Conversion of research reactors from HEU to LEU fuel. Fuel Cycle Waste Newsl 2 (1), 1–16.

Akaho, E.H.K., Nyarko, B.J.B., 2002. Characterization of neutron flux spectra in irradiation sites of MNSR reactor using Wescott-formalism for k0 neutron activation analysis method. Appl. Radiat. Isot. 57, 265–273.

Baidoo, I.K., 2012. Validation of IAEA K0-Instrumental Neutron Activation Analysis Software Using a Low Power Research Reactor GHARR-1. MPhil Thesis submitted to Department of Nuclear Science and Applications, Graduate School of Nuclear and Allied Sciences, University of Ghana.

Baidoo, I.K., Nyarko, B.J.B., Akaho, E.H.K., Dampare, S.B., Sogbadji, R.B.M., Poku, L.O., 2013. Characterization of low power research reactor neutrons for the validation of k0-INAA standardization based on k0-IAEA software. Appl. Radiat. Isot. 79, 85–93.

Chand, M., Rao, J.S.B., Samanta, S.K., Shekhawat, R.S., Senthilvadivu, R., Kumar, G.V.S. A., Kumar, R., 2022. Performance of various mathematical functions for the in-situ relative detector efficiency towards its applicability for k0 IM-NAA. Appl. Radiat. Isot. 184, 110194. https://doi.org/10.1016/j.apradiso.2022.110194.

Cui, T., Yang, Y., 2023. Yield calculation for delayed gamma-ray neutron activation analysis. Nucl. Instrum. Methods Phys. Res. A. https://doi.org/10.1016/j.nima.2023.168380.

De Corte, F., Simonits, A., 2003. Recommended nuclear data for use in the k0 standardization of neutron activation analysis. Atomic Data Nucl. Data Tables 85, 47–67. https://doi.org/10.1016/S0092-640X(03)00036-6.

De Corte, F., et al., 1979. Modification and generalization of some methods to improve the accuracy of α-determination in the 1/E1+α epithermal neutron spectrum. J. Radioanal. Nucl. Chem. 52 (2), 305–317.

De Corte, F., et al., 1987a. Accuracy and applicability of the k0-standardization method. J. Radioanal. Nucl. Chem. 113 (1), 145–161.

De Corte, F., et al., 1987b. Accuracy and applicability of the k0-standardization method. J. Radioanal. Nucl. Chem. 113 (1), 145–161.

Franek, M., Krivan, V., 1993. Multi-element analysis of aluminium-based ceramic powders by instrumental and radiochemical neutron activation analysis. Anal. Chim. Acta 282, 199–207.

Hamidatou, L.A., Dekar, S., Boukari, S., 2012. k0-NAA quality assessment in an Algerian laboratory by analysis of SMELS and four IAEA reference materials using Es-Salam research reactor. Nucl. Instrum. Methods Phys. Res. 682, 75–78. https://doi.org/10.1016/j.nima.2012.04.042.

Hien, N.T., Do, N.V., Kim, G., Naik, H., Khue, P.D., 2023. Measurement of neutron capture cross sections for the 174Yb(n,γ) 175Yb reaction at thermal and epithermal energies. Radiat. Phys. Chem. 205, 110738 https://doi.org/10.1016/j.radphyschem.2022.110738.

IAEA, 1970. Neutron Fluence Measurements, Technical Report No. 107. IAEA, Vienna, pp. 1–200.

IAEA, 1990a. Practical Aspects of Operating a Neutron Activation Analysis Laboratory. A Technical Document issued by the International Atomic Energy Agency, Vienna.

IAEA, 1990b. Practical Aspects of Operating a Neutron Activation Analysis Laboratory. IAEA-TECDOC-564, IAEA, Vienna, pp. 1–251.

Jovanovic, S., Vukotic, P., Smodis, B., Jacimovic, R., Mihaljevic, N., Stegnar, P., 1988. Epithermal neutron flux characterization of the TRIGA MARK II reactor, Ljubljana, Yugoslavia, for use in NAA. J. Radioanal. Nucl. Chem. 129, 343–349.

Karadag, M., Yucel, H., Tan, M., Ozmen, A., 2003. Measurement of thermal neutrons and resonance integral for 71Ga(n,γ) 72Ga and 75As(n,γ) 76As by using 241Am–Be isotopic neutron source. Nucl. Instrum. Methods Phys. Res. 501, 524–535.

Khattab, K., 2007. Measurement of fast neutron flux in the MNSR inner irradiation site. Appl. Radiat. Isot. 65, 46–49.
Kubešová, M., Kucera, J., 2012. How to calculate uncertainties of neutron flux parameters and uncertainties of analysis results in k0-NAA. J. Radioanal. Nucl. Chem. 293, 87–94. https://doi.org/10.1016/j.nima.2011.06.097, 2012.
Kuběsova', M., Kučera, J., 2011. Comparison of Kayzero for Windows and k0-IAEA software packages for k0 standardization in neutron activation analysis. Nucl. Instrum. Methods A 654, 206–212. https://doi.org/10.1016/j.nima.2011.06.097.
Kumar, G.V.S.A., Sen, S., Radh, E., Rao, J.S.B., Acharya, R., Kumar, R., Venkatasubramani, C.R., Reddy, A.V.R., M. Joseph, M., 2017. Studies on neutron spectrum characterization for the pneumatic fast transfer system (PFTS) of KAMINI reactor. Appl. Radiat. Isot. 124, 49–55.
Mensimah, E., Abrefah, R.G., Nyarko, B.J.B., Fletcher, J.J., Asamoah, M., 2011. Neutron flux determination in irradiation sites of an Am-Be neutron source at NNRI. Ann. Nucl. Energy 38, 2303–2308.
Nyarko, B.J.B., 2006. Development of Instrumental Neutron Activation Analysis Methods for the Assessment of Iodine and Selected Elements in Ghanaian Foods Using Low-Power Research Reactors. PhD Thesis. submitted to Department of Physics, Faculty of Science, University of Cape Coast.
Osei, B., 2017. Characterization of Ghana Research Reactor-1 Low Enriched Uranium Core Irradiation Sites Using a Theoretical Method. MPhil Thesis submitted to the Graduate School of Nuclear and Allied Sciences, University of Ghana, Legon, pp. 1–118.
Osei, B., Baidoo, I.K., Odoi, H.C., Gasu, P.D., Nyarko, B.J.B., 2021. The low enriched uranium miniature neutron source reactor (LEU-MNSR) neutron spectrum characterization for k0-INAA. Nucl. Instrum. Methods Phys. Res. A 1005, 165397.
Osmani, N., Benkharfia, H., Saad, D., 2023. Neutron-induced damage simulations using MCNP6 and SRIM codes: beyond neutron transmutation doping of silicon. Ann. Nucl. Energy 187, 109795. https://doi.org/10.1016/j.anucene.2023.109795, 2023.
Pomme, S., Hardeman, F., Robouch, P., Etxebarria, N., Arana, G., 1997. Neutron Activation Analysis with K0-Standardisation: General Formalism and Procedure. Nuclear Spectrometry Radiation Protection Department, SCKCEN, pp. 1–110. BLG-700, September 1997.
Rodriguez, D.C., Abbas, K., Koizumi, M., Nonneman, S., Rossi, F., Takahashi, T., 2021. Development and testing of a Delayed Gamma-ray Spectroscopy instrument utilizing Cf-252 neutrons evaluated for nuclear safeguards applications. Nucl. Instrum. Methods Phys. Res. A 1014, 165685. https://doi.org/10.1016/j.nima.2021.165685, 2021.
Salahi, S., Dorostkar, M.M., Saray, A.A., 2022. Measurement of deuterium concentration in heavy water utilizing prompt gamma neutron activation analysis (PGNAA) in comparison with MCNPX simulation results. Nucl. Eng. Technol. 54, 4231e4235 https://doi.org/10.1016/j.net.2022.06.021.
Samanta, S.K., Sengupta, A., Acharya, R., Pujar, P.K., P, K., 2021. Standardization and validation of k0-based Neutron Activation Analysis using Apsara-U reactor and its application to pure iron metal and coal sample for trace element determination. Nucl. Instrum. Methods Phys. Res. A 1018, 165856. https://doi.org/10.1016/j.nima.2021.165856.
Schlünz, E.B., Bokov, P.M., Prinsloo, R.H., van Vuuren, R.H., 2016. A unified methodology for single- and multiobjective in-core fuel management optimisation based on augmented Chebyshev scalarisation and a harmony search algorithm. Ann. Nucl. Energy 87, 659–670. https://doi.org/10.1016/j.anucene.2015.09.023.
Sidi-Ali, K., Medouri, E.M., Ailem, D., Mazidi, S., 2023. Neutronic calculations and thermal hydraulic application using CFD for the nuclear research reactor NUR at steady state mode. Prog. Nucl. Energy 159, 104640. https://doi.org/10.1016/j.pnucene.2023.104640.
Sogbadji, R.B.M., Nyarko, B.J.B., Akaho, E.H.K., Abrefah, R.G., 2011. Determination of neutron fluxes and spectrum shaping factors in irradiation sites of Ghana's miniature neutron source reactor (MNSR) by activation method after compensation of loss of excess reactivity. World J. Nucl. Sci. Technol. 1, 50–56.
van Sluijs, R., Jacimovic, R., Kennedy, G., 2014. A Simplified Method to Replace the Westcott Formalism in K0-NAA Using Non-1/v Nuclides. Akade'miai Kiado', Budapest, Hungary, 2014.

Glossary

Symbol Meaning (Unit)

GAEC: Ghana Atomic Energy Commission
GHARR-1: Ghana Research Reactor −1
HEU: High Enriched Uranium
LEU: Low Enriched Uranium
IAEA: International Atomic Energy Agency
MCNP: Monte Carlo N-Particle Simulation
MNSR: Miniature Neutron Source Reactor
NAA: Neutron Activation Analysis
SAR: Safety Analysis Report
SRM: Standard Reference material
CRM: Certified reference Material
w: Amount of element **(g)**
θ: Isotopic abundance
N_{av}: Avogadro's number **($[mol]^{-1}$)**
M: Atomic mass **($g.[mol]^{-1}$)**
φ: Effective neutron flux **($[ncm^{-2}s^{-1}]$)**
γ: Absolute gamma-ray abundance
ε: Absolute photopeak efficiency of the detector
S: Saturation correction
D: Decay correction
C: Counting correction
λ: Decay constant of the activated nuclide
ρ: Concentration **($[g/g]$)**
t_r: Irradiation time **(s)**
t_d: Decay time **(s)**
t_c: Counting time **(s)**
A_{sp}: Specific counting rate **($[s^{-1}g^{-1}]$)**
I_0: Resonance integral cross-section **(b)**
α: Epithermal neutron shaping factor
f: Thermal/epithermal flux ratio
σ_0: Thermal neutron capture cross-section **($[ncm^{-2}s^{-1}]$)**
$Q_0(I_0/\sigma_0)$: Ideal resonance integral/thermal neutron cross-section ratio
$Q_0(\alpha)$: Non-ideal resonance integral to thermal neutron cross-section
F_{cd}: Cadmium transmission factor
R_{Cd}: Cadmium ratio
G_{th}: Thermal neutron self-shielding factor
G_{epi}: Epithermal neutron self-shielding factor
A_{bare}: Specific activities obtained after irradiation of a bare foil **(Bq)**
A_{cd}: Specific activities obtained after irradiation Cd covered foil **(Bq)**
N_t: Net count under the full energy peak during an acquisition time of t
N_0: Initial number of atoms of the nuclide to be activated
φ_f: Fast neutron flux **($[ncm^{-2}s^{-1}]$)**
φ_{epi}: Epithermal neutron flux density **($[ncm^{-2}s^{-1}]$)**
φ_{th}: Thermal neutron flux density **($[ncm^{-2}s^{-1}]$)**
E_r: The effective resonance energy
v_{Cd}: Neutron velocity corresponding to E_{Cd}
E_{Cd}: Cadmium cut off energy 0.55eV
$1/E^{1+\alpha}$: Defines the shape of the epithermal neutron spectrum
ISE: International Soil-Analytical Exchange
PT_19: PTNATIAEA19
RRD: Research Reactor Database